ELSEVIER

Materials Science and Engineering A332 (2002) 1–10

MATERIALS SCIENCE & ENGINEERING A

www.elsevier.com/locate/msea

Phase transformation in AISI 410 stainless steel

M.C. Tsai *, C.S. Chiou [1], J.S. Du [2], J.R. Yang

Institute of Materials Science and Engineering, National Taiwan University, 1 Roosevelt Rd., Sec. 4, Taipei, Taiwan, ROC

Received 9 April 2001

Abstract

AISI 410 stainless steel can virtually fully transform to dislocated lath martensite at a very low cooling rate by air cooling. It is found that at the same cooling rate the specimen austenitized at the higher temperature has a lower martensite start temperature (Ms); besides, the difference of Ms becomes much larger at the higher cooling rate. In the continuously cooled specimens investigated, significant amounts of inter-martensite retained austenite film may be imaged, where the martensite laths tend to be in the same crystallographic orientation. On the other hand, micro-twinning is generally detected in martensite laths when the adjacent variants of martensite form in a twin-related manner. Another important result indicates that no bainitic structure can be obtained in this steel for the isothermal transformation just above the martensitic start temperature (Ms), and suggests that the single C curve in the time–temperature–transformation (TTT) diagram of AISI 410 is for a diffusional transformation. The prior heavy deformation of austenite also gives strong evidence to suggest that severe deformation causes mechanical stabilization of austenite against martensitic transformation.

Keywords: Martensitic stainless steel; Continuous cooling transformation; Ms temperature; Retained austenite; Micro-twinning; Isothermal transformation; Mechanical stabilization

1. Introduction

In low alloy steels, the pearlitic and bainitic temperature ranges overlap each other to a considerable extent, and this make the interpretation of microstructure and kinetics very difficult. However, in medium alloy steels, the isothermal time–temperature–transformation (TTT) diagram possesses two C curves [1,2]. In such a diagram, the upper C curve represents the time taken for the initiation of diffusional transformation such as allotriomorphic ferrite and pearlite, whereas the lower C curve represents the time taken for the initiation of displacive transformation such as bainite [3,4]. On the other hand, in commercial martensitic stainless steels, the TTT diagram possesses single C curve only. In this respect, Bhadeshia had used the concepts of nucleation of ferrite (which exhibited an invariant plane strain) and stored energy due to shape change, and proposed a thermodynamic model to explain why the bainitic transformation does not occur in these high alloy steels [3]. However, there was no experimental work on the isothermal transformation just above the Ms temperature for these high alloy steels to elucidate whether the bainitic transformation can occur or not. An attempt in this work is therefore to justify the above outstanding claim.

AISI 410 stainless flsteel is the progenitor in the commercial low-carbon martensitic stainless steels, and is widely used in many industries for the essential parts (such as parts for HDD, plastic moulds, screws for extruder, valves, shafts and bearings) due to its corrosion-resistance, high strength and high toughness. The study of retained austenite and martensitic structure in this type of martensitic steels has assumed great significance, due to their influence on the mechanical properties. There was extensive research work [5–11] in the 1970's on retained austenite, twinned plate martensite and lath martensite in alloy steels. In order to fully understand the martensitic transformation and existence of retained austenite in this steel, a series of continuous cooling treatment, isothermal treatment and

* Corresponding author.
E-mail address: jryang@ccms.ntu.edu.tw (M.C. Tsai).
[1] Present address: Department of Mechanical Engineering, Yuan-Ze University, Chung-Li, Taoyuan, Taiwan, ROC.
[2] Present address: Applied Materials Twain Co., Hsin-Chu, Taiwan, ROC.

0921-5093/02/$ - see front matter
PII: S0921-5093(01)01710-5

Table 1
Chemical composition of the steel (wt.%)

Fe	C	Cr	S	Mo	Si	Cu	Sn	Mn	Ni	Al	N	P
Balance	0.12	12.80	0.006	0.02	0.33	0.04	0.01	0.44	0.12	0.01	0.031	0.023

thermomechanical treatment have been carried out on a Dilatronic III dilatometer of Theta Industries, Inc. The dilatometric curves, optical metallographs and transmission electron micrographs have been examined to elucidate the microstructural development. Furthermore, the effects of austenitizing temperature and cooling rate on Ms temperature have been investigated. The interpretations for the observed phenomena have been proposed.

2. Experimental procedure

A commercial AISI 410 steel bar with 16 mm diameter in the annealed state was used as the starting material. The steel was produced by Gloria Material Technology Corporation through the process of electric arc furnace melting, vacuum ladle furnace treatment, ingot casting, forging, rolling and annealing. The chemical composition of the steel studied is listed in Table 1.

In this work, all the thermal treatments have been carried out on a Dilatrometric III RDP deformation dilatometer of Theta Industries, Inc. Before preparation for dilatrometric specimens, the pieces of steel plate were homogenized at 1200 °C for 3 days, then quenched into water, and finally removed the decarburization layer. The specimens were machined in the form of 3 mm diameter cylindrical rods with 6 mm length. The experiments included three parts as described in the following.

1. Continuous cooling treatment. The processing scheme performed in the dilatometer is presented in Fig. 1a; the dilatometer specimens were austenitized at 900, 1000, 1100, 1200 °C for 10 min, and then cooled at different cooling rates (0.5–100 °C s^{-1}) to room temperature.
2. Isothermal treatment. The specimens were heated to 1000 °C for 10 min, and then rapidly cooled to the temperature range 370–600 °C for isothermal transformation. The schematic diagram for isothermal treatment is shown in Fig. 1b.
3. Thermomechanical treatment. After austenitization at 1000 °C for 10 min, the specimens were cooled to 750 °C at a cooling rate of 60 °C s^{-1}, immediately, different amounts (0, 10, 20 and 40%) of compressive deformation were executed within 3 s. After deformation, the specimens were held at 290 °C for isothermal treatment until the transformation was completed, and immediately rapidly up-quenched to 350 °C for tempering the existing martensite. The schematic diagram for thermomechanical treatment is shown in Fig. 1c.

The transmission electron microscopy samples were prepared from 0.25 mm thick discs cut from the dilatometer specimens. The discs were thinned to 0.05 mm by abrasion on silicon carbide papers and then twin-jet electropolished using a mixture of 5% perchloric acid, 25% glycerol and 70% ethanol at ambient

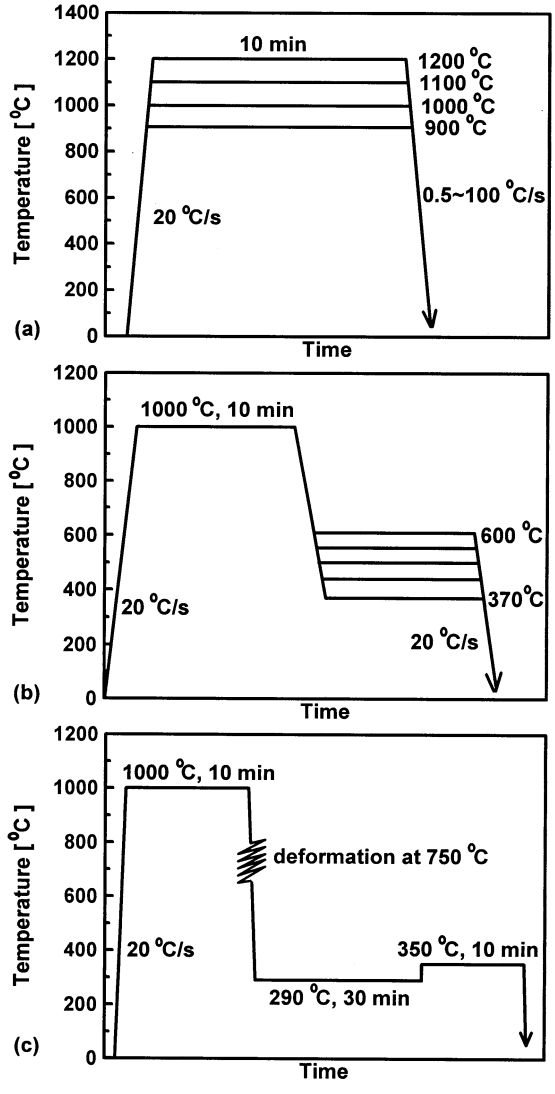

Fig. 1. Schematic diagrams showing the processing performed in the dilatometer, (a) continuous cooling treatment; (b) isothermal treatment; (c) thermomechanical treatment.

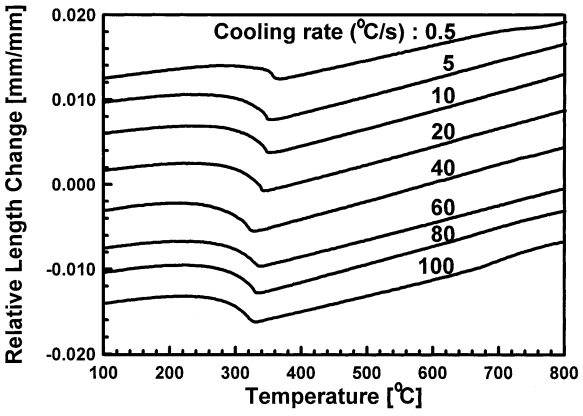

Fig. 2. The dilatometric curves for the specimen austenitized at 900 °C for 10 min followed by cooling at 0.5–100 °C s^{-1}.

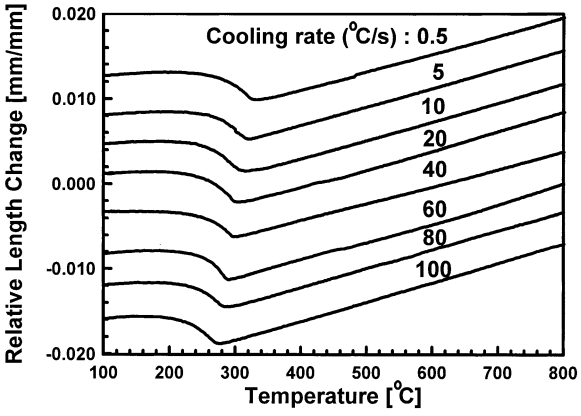

Fig. 3. The dilatometric curves for the specimen austenitized at 1000 °C for 10 min followed by cooling at 0.5–100 °C s^{-1}.

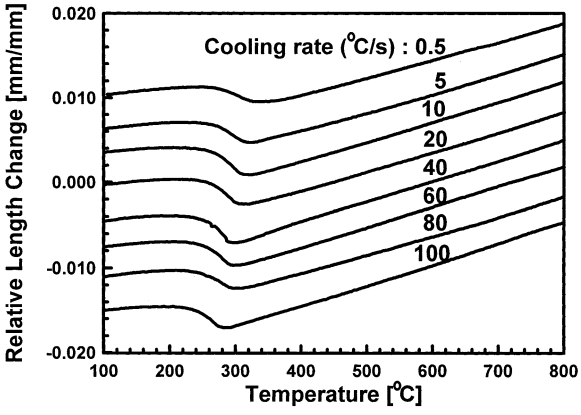

Fig. 4. The dilatometric curves for the specimen austenitized at 1100 °C for 10 min followed by cooling at 0.5–100 °C s^{-1}.

temperature and 60 V polishing potential. They were examined using a JEOL 100CX transmission electron microscope operating at 100 kV.

3. Results and discussion

In order to investigate the effects of cooling rate on Ms temperature in AISI 410 stainless steel, a series of continuous cooling treatment has been done. Fig. 2 shows the dilatometric curves for the specimens austenitized at 900 °C for 10 min and followed by the cooling at different rates (0.5–100 °C s^{-1}). It is obvious that

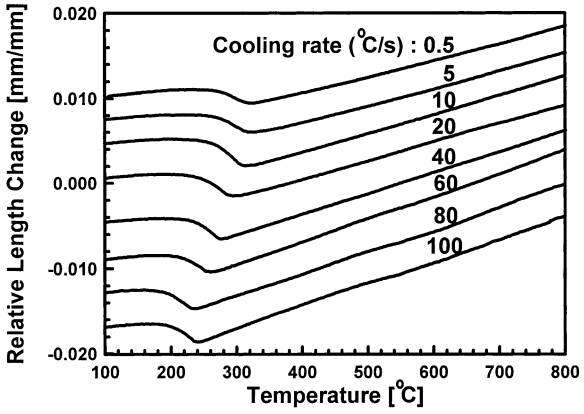

Fig. 5. The dilatometric curves for the specimen austenitized at 1200 °C for 10 min followed by cooling at 0.5–100 °C s^{-1}.

Table 2
The Ms temperature measured from dilatometric curves

Cooling rate (°C s^{-1})	Austenitization temperature			
	900 °C	1000 °C	1100 °C	1200 °C
0.5	375	360	355	340
5	360	340	340	335
10	350	335	335	330
20	345	320	320	315
40	340	300	300	290
60	335	295	290	270
80	330	290	285	250
100	320	285	280	245

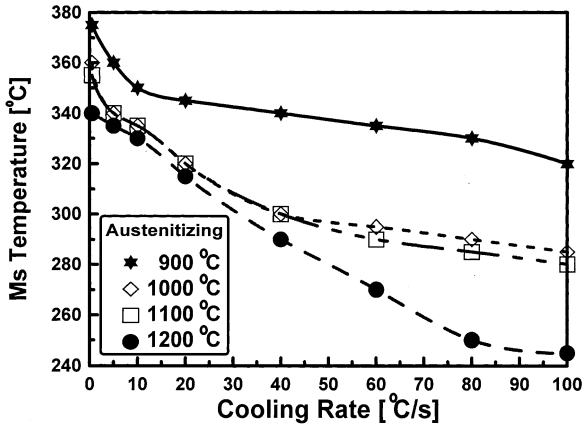

Fig. 6. Plot of Ms vs. cooling rate for four different austenitization temperatures.

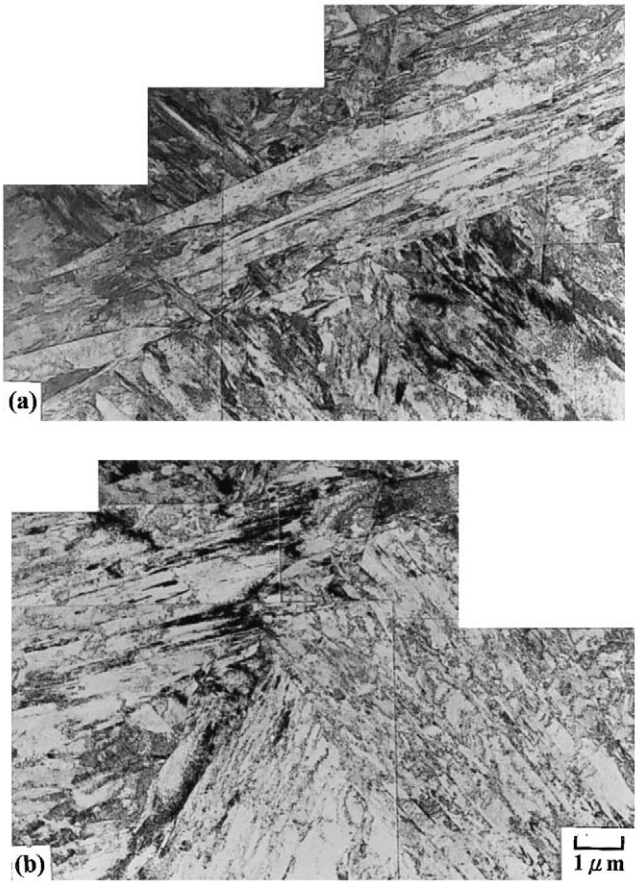

Fig. 7. TEM obtained from the specimens austenitized at 1000 °C followed by continuous cooling at (a) 0.5 and (b) 100 °C s^{-1}.

the Ms temperature decreases with increasing cooling rate. The similar phenomena were also found for the specimens austenitized at 1000, 1100 and 1200 °C as shown in Figs. 3–5.

The Ms temperatures have been measured (as presented in Table 2) from the dilatometric curves in Figs. 2–5 for different austenitization temperature conditions with a wide range of cooling rate. The Ms temperature versus cooling rate is plotted in Fig. 6. It indicates that at the same cooling rate the specimen with the higher

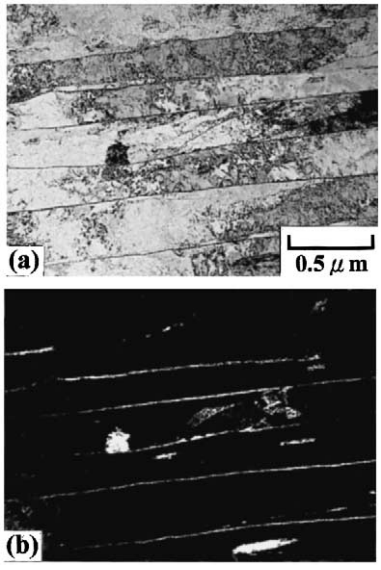

Fig. 9. Bright and dark field images of TEM for retained austenite films obtained from the specimen continuously cooled at 100 °C s^{-1} after austenitization at 1100 °C for 10 min.

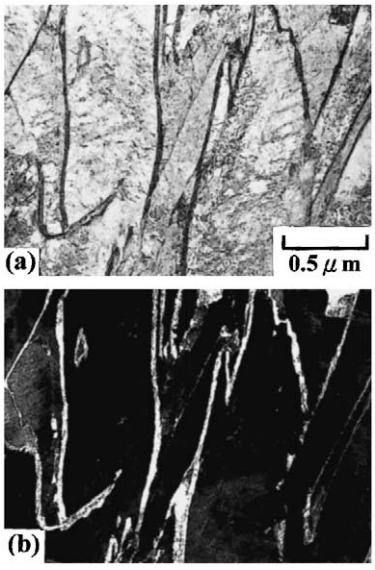

Fig. 8. Bright and dark field images of TEM for retained austenite films obtained from the specimen continuously cooled at 0.5 °C s^{-1} after austenitization at 1100 °C for 10 min.

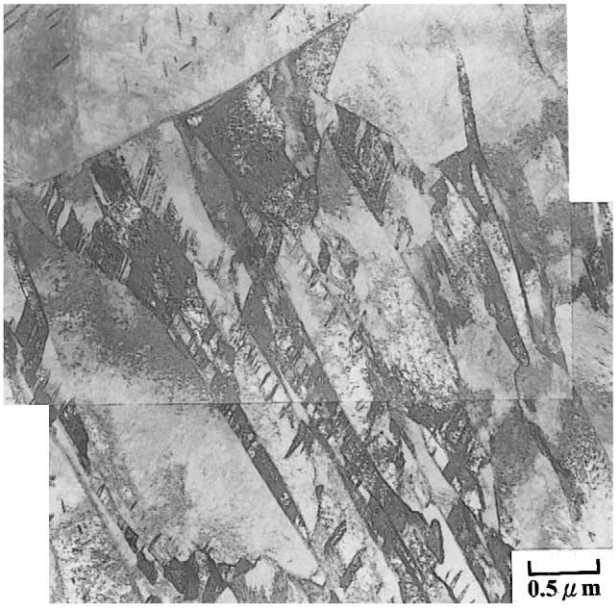

Fig. 10. Transmission electron micrograph obtained from the specimen continuously cooled at 0.5 °C s^{-1} after austenitization at 1100 °C for 10 min.

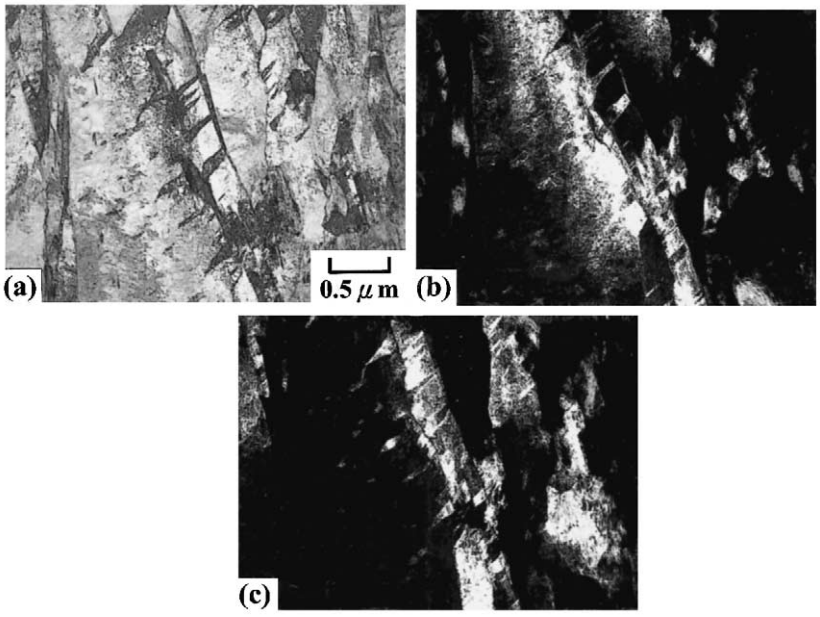

Fig. 11. Micro-twins in AISI 410 steels obtained from specimens cooling at 0.5 °C s^{-1}, (a) bright field micrograph; (b) dark field of left side martensitic lath; (c) dark field of right side martensitic lath.

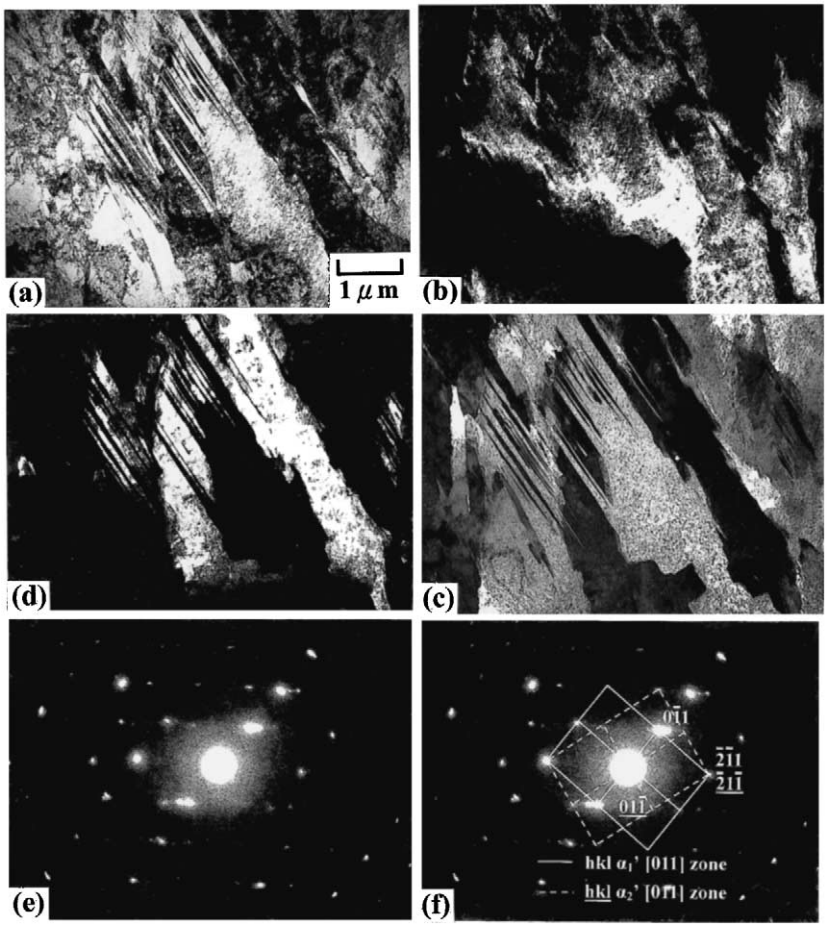

Fig. 12. Micro-twins in AISI 410 steels obtained from specimens cooling at 100 °C s^{-1}, (a) bright field image; (b) dark field image using $(\bar{2}\bar{1}1)$ reflection; (c) dark field image using α_1' $(0\bar{1}1)$ reflection; (d) dark field image using α_2' $(01\bar{1})$ reflection; (e) corresponding diffraction pattern; (f) interpretation of (e).

Table 3
Twenty-four equivalent axis–angle pairs relating twinning within the martensitic laths

Number	The 23 equivalent axis–angle pairs			
	Axis			Angle
1	0	0.7071	0.7071	70.5
2	0.4082	0.8165	0.4082	180
3	0.7071	0.7071	0	70.5
4	0.5774	0.5774	0.5774	180
5	−0.9045	0.3015	0.3015	146.4
6	−0.3015	−0.3015	0.9045	146.4
7	−0.7071	−0.7071	0	109.5
8	−0.5774	0.5773	−0.5774	60
9	0.3015	0.9045	−0.3015	146.4
10	0.4082	0.4082	0.8165	180
11	0.8944	−0.4472	0	131.8
12	0.4472	0	0.8944	131.8
13	0.7071	0	−0.7071	109.5
14	0.9045	0.3015	0.3015	146.4
15	−0.3015	−0.3015	−0.9045	146.4
16	−0.7071	0	0.7071	70.5
17	0	−0.8944	0.4472	131.8
18	−0.4472	0.8944	0	131.8
19	0.3015	−0.9045	−0.3015	146.4
20	0	0.7071	0.7071	109.5
21	0.5774	−0.5774	0.5773	60
22	0	0.4472	−0.8944	131.8
23	−0.8944	0	−0.4472	131.8
24	0.8165	0.4082	0.4082	180

Table 4
Twenty-four independent variants of the K–S orientation relationships

Variant number	Description	Group number
1	$(011)_{\alpha'}//(111)_{\gamma}$ $[\bar{1}\bar{1}1]_{\alpha'}//[\bar{1}01]_{\gamma}$	1
2	$(011)_{\alpha'}//(111)_{\gamma}$ $[\bar{1}\bar{1}1]_{\alpha'}//[\bar{1}01]_{\gamma}$	1
3	$(011)_{\alpha'}//(111)_{\gamma}$ $[\bar{1}\bar{1}1]_{\alpha'}//[0\bar{1}1]_{\gamma}$	1
4	$(011)_{\alpha'}//(111)_{\gamma}$ $[\bar{1}\bar{1}1]_{\alpha'}//[0\bar{1}1]_{\gamma}$	1
5	$(011)_{\alpha'}//(111)_{\gamma}$ $[\bar{1}\bar{1}1]_{\alpha'}//[1\bar{1}0]_{\gamma}$	1
6	$(011)_{\alpha'}//(111)_{\gamma}$ $[\bar{1}\bar{1}1]_{\alpha'}//[1\bar{1}0]_{\gamma}$	1
7	$(011)_{\alpha'}//(\bar{1}\bar{1}1)_{\gamma}$ $[\bar{1}\bar{1}1]_{\alpha'}//[1\bar{1}0]_{\gamma}$	2
8	$(011)_{\alpha'}//(\bar{1}\bar{1}1)_{\gamma}$ $[\bar{1}\bar{1}1]_{\alpha'}//[1\bar{1}0]_{\gamma}$	2
9	$(011)_{\alpha'}//(\bar{1}\bar{1}1)_{\gamma}$ $[\bar{1}\bar{1}1]_{\alpha'}//[101]_{\gamma}$	2
10	$(011)_{\alpha'}//(\bar{1}\bar{1}1)_{\gamma}$ $[\bar{1}\bar{1}1]_{\alpha'}//[101]_{\gamma}$	2
11	$(011)_{\alpha'}//(\bar{1}\bar{1}1)_{\gamma}$ $[\bar{1}\bar{1}1]_{\alpha'}//[011]_{\gamma}$	2
12	$(011)_{\alpha'}//(\bar{1}\bar{1}1)_{\gamma}$ $[\bar{1}\bar{1}1]_{\alpha'}//[011]_{\gamma}$	2
13	$(011)_{\alpha'}//(\bar{1}1\bar{1})_{\gamma}$ $[\bar{1}\bar{1}1]_{\alpha'}//[110]_{\gamma}$	3
14	$(011)_{\alpha'}//(\bar{1}1\bar{1})_{\gamma}$ $[\bar{1}\bar{1}1]_{\alpha'}//[110]_{\gamma}$	3
15	$(011)_{\alpha'}//(\bar{1}1\bar{1})_{\gamma}$ $[\bar{1}\bar{1}1]_{\alpha'}//[011]_{\gamma}$	3
16	$(011)_{\alpha'}//(\bar{1}1\bar{1})_{\gamma}$ $[\bar{1}\bar{1}1]_{\alpha'}//[011]_{\gamma}$	3
17	$(011)_{\alpha'}//(\bar{1}1\bar{1})_{\gamma}$ $[\bar{1}\bar{1}1]_{\alpha'}//[\bar{1}10]_{\gamma}$	3
18	$(011)_{\alpha'}//(\bar{1}1\bar{1})_{\gamma}$ $[\bar{1}\bar{1}1]_{\alpha'}//[\bar{1}01]_{\gamma}$	3
19	$(011)_{\alpha'}//(1\bar{1}\bar{1})_{\gamma}$ $[\bar{1}\bar{1}1]_{\alpha'}//[110]_{\gamma}$	4
20	$(011)_{\alpha'}//(1\bar{1}\bar{1})_{\gamma}$ $[\bar{1}\bar{1}1]_{\alpha'}//[110]_{\gamma}$	4
21	$(011)_{\alpha'}//(1\bar{1}\bar{1})_{\gamma}$ $[\bar{1}\bar{1}1]_{\alpha'}//[101]_{\gamma}$	4
22	$(011)_{\alpha'}//(1\bar{1}\bar{1})_{\gamma}$ $[\bar{1}\bar{1}1]_{\alpha'}//[101]_{\gamma}$	4
23	$(011)_{\alpha'}//(1\bar{1}\bar{1})_{\gamma}$ $[\bar{1}\bar{1}1]_{\alpha'}//[0\bar{1}1]_{\gamma}$	4
24	$(011)_{\alpha'}//(1\bar{1}\bar{1})_{\gamma}$ $[\bar{1}\bar{1}1]_{\alpha'}//[0\bar{1}1]_{\gamma}$	4

austenitization temperature has a lower martensite start temperature (Ms); besides, the difference of Ms becomes much larger at the higher cooling rate. The Ms temperatures for the specimens austenitized at 900, 1000, 1100 and 1200 °C separately and followed by cooling at 100 °C s^{-1} are determined to be 320, 285, 280 and 245 °C, respectively. It is noticed that at the cooling rate of 100 °C s^{-1}, Ms in the case with austenitization at 1200 °C is lower than that in the case with austenitization at 900 by 75 °C. The result provides strong evidence showing that the higher austenitization temperature with the higher cooling rate depresses the martensitic transformation.

Some related research work has been done by Hsu et al. [12] who claimed that values of Ms decreased with the increase of the quenching temperature above 900 °C in Fe–29Ni (wt.%), Fe–30Ni (wt.%) and Fe–31Ni (wt.%) alloys. They suggested that the pinning of clustered vacancies to the partial dislocations hindered the nucleation of martensite and consequently depressed the Ms temperature. The detailed research about interaction between vacancies and the edge dislocation in body centered cubic (b.c.c.) metal had been studied by Ingle et al. [13] The variation of Ms in Fe–C, Fe–Mn, Fe–Si, Fe–Ni–C and Fe–Cr–C [14] alloys have also been investigated through considering the strength of matrices. Because carbon atom has most powerful solid-solution strengthening effect on austenite than other alloying atoms (such as Cr, Ni and Si), it has been supposed to be the main element in steels to influence the Ms temperature. When the chromium carbide precipitates in matrix, the lower amount of carbon retained in solid-solution austenite would lead to a higher Ms temperature.

The possible factors to affect the Ms temperature can be listed as follows, (1) chemical composition in matrix; (2) grain size of austenite [15]; (3) cooling rate [16]; (4) crystal defect and inclusion [17,18]; (5) occurrence of other pre-transformations [19]; (6) stress and strain [20]; (7) magnetization [21]; (8) hydrostatic pressure. In this work, the factors (6)–(8) could be neglected. Generally, the main factor to influence the Ms temperature is the strength of parent austenite structure. If the strength of prior austenite is high, the Ms temperature will be depressed to a lower temperature. Factors (1) and (2) would be related with this main factor. For example, the increase in cooling rate could induce the larger quantities of vacancy in matrix to strength the austenite, and leads to a lower Ms temperature. On the other hand, the variation of Ms could be due to the difference in the grain size of austenite. The explanation for the grain size effect has been well known; the increased strength of austenite by grain refining makes it more difficult to accommodate plastically the shape strain of the transforming martensite plate, thus depressing the Ms temperature in fine-grained specimens. However,

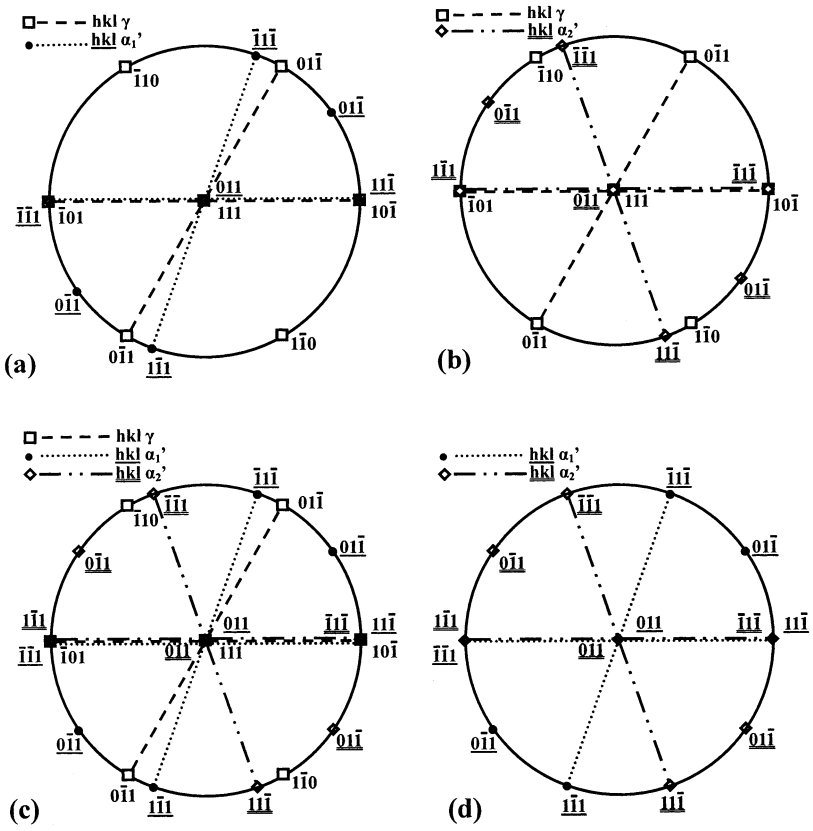

Fig. 13. The explanation of twin relative using stereograph, (a) KS orientation relationship for α'_1 with γ; (b) KS orientation relationship for α'_2 with γ; (c) superimposition of (a) and (b); (d) α'_1 and α'_2 being twin-related.

the plausible explanation in this work is suggested that the higher austenitization temperature with the higher cooling rate gives the austenite matrix with a higher concentration of vacancies and without any precipitation of chromium carbides. The increased strength of austenite by the interaction between dislocations and vacancies, and by the solid solution due to carbon and chromium elements preserved in the matrix leads to the lower Ms temperature.

The study of retained austenite and martensitic structure in this type of martensitic steels has assumed great significant, primarily due to their influence on mechanical properties of commercially used quenched and tempered ultra-high strength steels. However, the detailed microstructure development is still need to elucidate. Transmission electron micrographs with a low magnification in Fig. 7 were obtained from the specimens austenitized at 1000 °C and followed by continuous cooling at 0.5 and 100 °C s^{-1}, respectively, to room temperature. For the slow cooling rate condition (Fig. 7a), large laths of martensite partitioned the prior austenite grain and fine laths of martensite swamped the partitioned areas. On the other hand, for the high cooling rate condition (Fig. 7b), much more uniform fine laths of martensite could be obtained. The result implies that at a slow cooling rate, the martensite lath forms at the high temperature has enough time to grow without impingement with other martensite variants. Besides, auto-tempered martensite (with several variants of carbides) could be identified in the specimens treated by the slow continuous cooling. Bright and dark field images of transmission electron micrographs for retained austenite in the martensitic matrices were shown in Figs. 8 and 9, obtained from the specimen austenitized at 1100 °C and cooled at 0.5 and 100 °C s^{-1}, respectively. Significant amounts of inter-martensite retained austenite films could be detected and it was also found that the martensite laths tended to be in the same crystallographic orientation in space (over a distance of approximately six martensite laths at least). It was noted that the wider the lath of martensite, the thicker the film of retained austenite (as shown in Figs. 8 and 9). When the laths constituting a packet were in the same orientation, it was presumed that the shape deformation of each unit within the packet was identical. It is therefore suggested that mechanical stabilization, which essentially involves the jamming of the austenite–martensite interface by accommodation defects could be responsible for the stability of the austenite films.

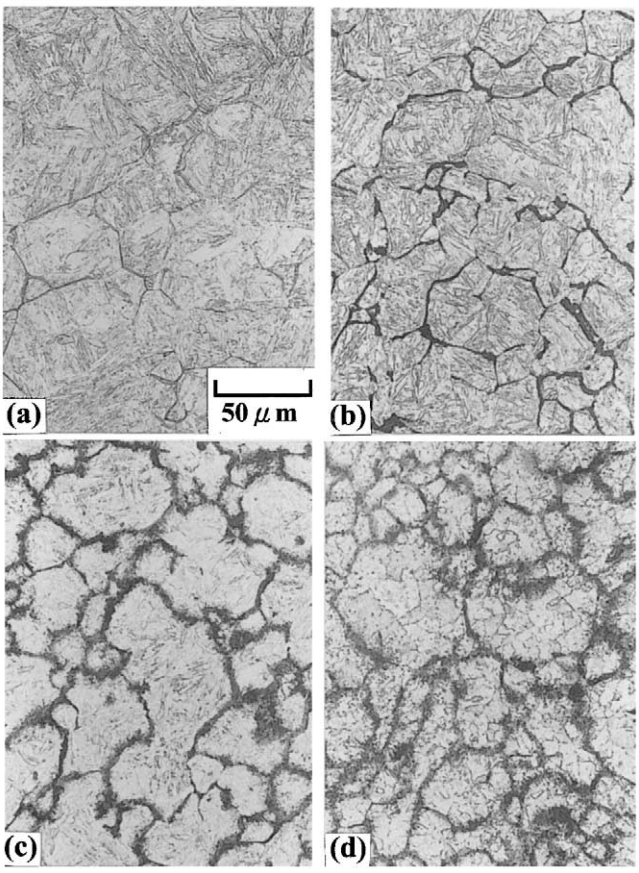

Fig. 14. Optical metallographs showing the specimens isothermally treated at 600 °C for various periods of time, (a) 1 h; (b) 4 h; (c) 8 h; (d) 16 h.

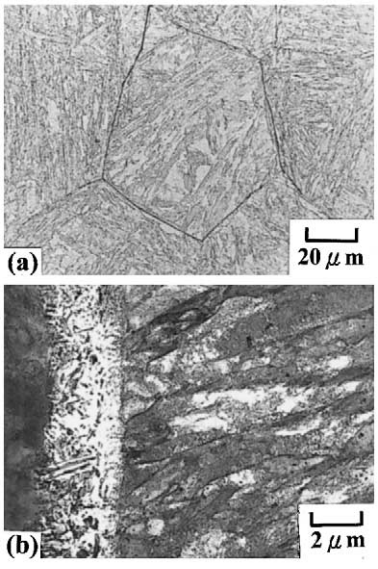

Fig. 15. (a) Optical micrographs and (b) transmission electron micrograph obtained from the specimen tempered at 370 °C for 11 days.

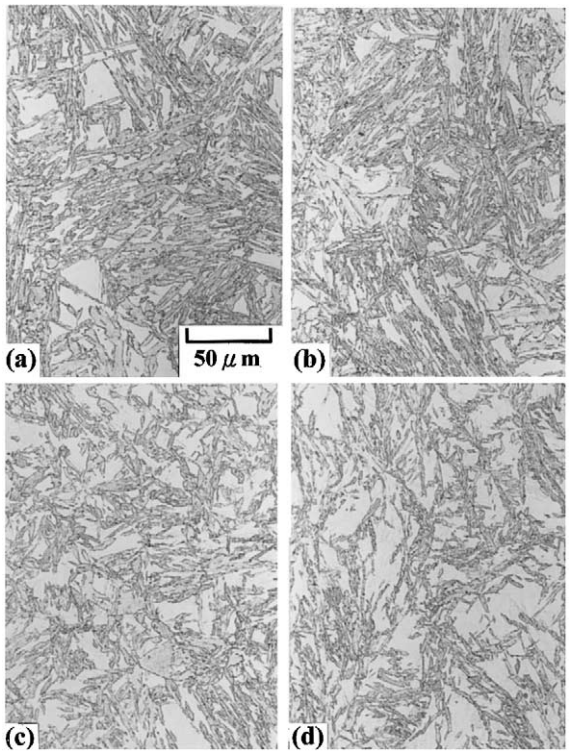

Fig. 16. The optical microscope microstructure by austenitizing to 1000 °C and given 0–40% deformation at 750 °C, then hold temperature at 290 °C, (a) 0%; (b) 10%; (c) 20%; (d) 40%.

Martensitic structure is normally considered to give dislocated laths if carbon content of the steel is less than 0.4 wt.%. However, it has been frequently found that micro-twins exist within the martensite laths (as shown in Fig. 10) in this steel. To resolve the mechanism of twin formation, before attempting to study the effect of twinning on the mechanical properties, is important. Although AISI 410 steel has a high Ms over room temperature, micro-twinning could often be observed in martensite laths. These twins extended partially cross the martensite units and the inter-twin spacing were generally large; these features are different from those in twinned plate martensite. Examination of bright field, diffraction patterns and dark field images (Figs. 11 and 12) found that micro-twinning was extensive when adjacent martensite laths were twin related, and that these interpenetrating twins had the same orientation with the adjacent martensite lath. It was apparent that the formation of these kinds of twins resulted from the high degree of mutually compensating accommodation between twin related martensite variants. Such micro-twins were not intrinsic transformation features. Table 3 shows the 24 equivalent axis–angle pairs for twins calculated from electron diffraction patterns of Fig. 12f.

The prevalent orientation relationships describing the austenite and martensite disposition after transformation can be listed as follows [22].

Kurdjumov–Sachs (KS) $(111)_\gamma//(011)_{\alpha'}$ $[\bar{1}01]_\gamma//[\bar{1}\bar{1}1]_{\alpha'}$.
Greninger–Troiano (GT) $(111)_\gamma$ 0.2° from $(011)_{\alpha'}$ $[\bar{1}01]_\gamma$ 2.7° from $[\bar{1}\bar{1}1]_{\alpha'}$.
Nishiyama–Wasserman (NW) $(111)_\gamma//(011)_{\alpha'}$ $[\bar{1}01]_\gamma//[100]_{\alpha'}$.

Considering the KS orientation relationship, 24 independent crystallographic variants of martensite can be obtained within a single crystal of austenite as shown in Table 4. Four groups can be assigned to the four independent $\{111\}_\gamma$ planes in a given austenite crystal. In each group, six independent variants can be obtained by ration about the pole of $(011)_{\alpha'}//\{111\}_\gamma$. Hence, for four groups 24 independent variants exist. The 24 KS relationships have the special property that variants of martensie can be twin-related in pairs (such as variants 1–2, 3–4, 5–6, …). It can be illustrated as follows. Fig. 13a and b show variants 1 and 2 of martensite with their respective KS orientation relationship. It is clear that variants 1–2 have the twin-related orientation (Fig. 13d). Similarly, variants 3–4, 5–6, 7–8, and so on are twin-related. It is found that twin related variants cannot be obtained by choosing variants from different groups. The twin-related orientation happens in only 12 combinations out of 276. Bhadeshia examined the crystal orientations for NW and GT relationships, and claimed that for NW and GT relationships, the adjacent laths of martensite can not have twin-related orientation [23]. It is suggested that micro-twins in lath martensite structure depends on the local crystallography.

It had been well know that the AISI 410 stainless steel only has single C curve in the TTT diagram [24]. Bhadeshia [3] has proposed a thermodynamic mode to explain the bainitic transformation does not occur in this steel. Fig. 14 illustrates the microstructures obtained from the specimens after completion of isothermal transformation at 600 °C for 1, 4, 8 and 16 h. The optical micrographs show a thin diffusion layer of carbide decorated at prior austenite grain boundaries. Examination of a specimen isothermally transformed slightly above the Ms temperature, at 370 °C, for 11 days (before finally quenching to ambient temperature) revealed that alloy-pearlite formed along martensite grain boundaries (Fig. 15). No bainitic structure could be identified and there was no evidence for bainitic transformation in this alloy steel. The result is consistent with that proposed by Bhadeshia, and strongly indicates that the single C curve in the TTT diagram of AISI 410 is for a diffusional transformation.

Optical metallographs in Fig. 16 were obtained from the specimens after austenitization at 1000 °C for 10 min, followed by different amounts of prior deformation (0, 10, 20 and 40%) at 750 °C, followed by isothermal transformation at 290 °C for 30 min (i.e. the time is longer enough to complete the isothermal transformation), and then up-quenched to 350 °C in order to temper the existing martensite. The metallographs in Fig. 16 are illustrated as follows. The grey etching regions represented the martensite, which formed and was immediately tempered after isothermal treatment (grey etching structure was due to the existence of interlath carbides within martensite). The white etching regions represented the martensite, which formed during cooling to room temperature after up-quench treatment. They show an increase in difficulty of martensite lath propagation into the austenite phase due to work hardening of austenite. This phenomenon elucidates severe deformation leads to mechanical stabilization of austenite against martensitic transformation.

4. Conclusion

An investigation has been made of the phase transformations in AISI 410 stainless steel. Based on the study of dilatometry, optical metallography and transmission electron microscopy, the following conclusion were drawn.

The results show that the Ms temperature decreases with the increase of cooling rate, and that at the same cooling rate the specimen austenitized at the higher temperature has a lower Ms temperature. The plausible explanation is suggested that the austenite matrix with a higher concentration of vacancies and a lack of chromium carbide precipitation leads to a lower Ms temperature.

The existence of retained austenite films and micro-twins in lath martensite structure depends on the local crystallography, which results in mechanical stabilization of austenite films or mechanical accommodation of interpenetrating twins.

Examination of isothermal transformation just above Ms temperature confirms that the single C curve in the TTT diagram of AISI 410 stainless steel is for a diffusional transformation.

Heavy deformation of prior austenite causes mechanical stabilization of the austenite and leads to the difficulty of martensite lath propagation into the austenite.

Acknowledgements

This work was carried out with financial support from the National Science Council of the Republic of China, Taiwan, under Contract NSC 88-2216-E-002-037.

References

[1] H.K.D.H. Bhadeshia, Acta Metall. 29 (1981) 1117–1130.
[2] A. Ali, H.K.D.H. Bhadeshia, Mater. Sci. Technol. 6 (1990) 781–784.

[3] H.K.D.H. Bhadeshia, Bainite in Steels, The Institute of Materials, London, 1992, pp. 126–133.
[4] A. Ali, H.K.D.H. Bhadeshia, Mater. Sci. Technol. 7 (1991) 895–903.
[5] S.K. Das, G. Thomas, Metall. Trans. 1 (1970) 325–327.
[6] D.H. Huang, G. Thomas, Metall. Trans. 2 (1971) 1587–1598.
[7] M. Raghavan, G. Thomas, Metall. Trans. 2 (1971) 3433–3439.
[8] G.Y. Lai, W.E. Wood, R.A. Clark, V.F. Zackay, E.R. Parker, Metall. Trans. 5 (1974) 1663–1670.
[9] E.R. Parker, Metall. Trans. A 8A (1977) 1025–1042.
[10] G. Thomas, Metall. Trans. A 9A (1978) 439–450.
[11] K.H. Khan, W.E. Wood, Metall. Trans. A 9A (1978) 899–907.
[12] T.Y. Hsu, Y. Linfah, J. Mater. Sci. 18 (1983) 3213–3218.
[13] K.W. Ingle, A.G. Crocker, Acta Metall. 26 (1978) 1461–1469.
[14] T.Y. Hsu, J. Mater. Sci. 20 (1985) 23–31.
[15] S. Kajiwara, Metall. Trans. A 17A (1986) 1693–1702.
[16] J.C. Brachet, L. Gavard, C. Boussidan, C. Lepoittevin, S. Denis, C. Servant, J. Nucl. Mater. 258–263 (1998) 1307–1311.
[17] J.W. Brooks, M.H. Loretto, R.E. Smallman, Acta Metall. 27 (1979) 1829–1838.
[18] J.W. Brooks, M.H. Loretto, R.E. Smallman, Acta Metall. 27 (1979) 1839–1847.
[19] A. Alamo, J.C. Brachet, A. Castaing, C. Lepoittevin, F. Barcelo, J. Nucl. Mater. 258–263 (1998) 1228–1235.
[20] S. Kajiwara, Mater. Trans. JIM 33 (1992) 1027–1034.
[21] T. Kakeshita, T. Saburi, K. Shimizu, Mater. Sci. Eng. A273–A275 (1999) 21–39.
[22] H.K.D.H. Bhadeshia, Ph.D. thesis, University of Cambridge, 1979.
[23] H.K.D.H. Bhadeshia, Worked Examples in the Geometry of Crystals, The Institute of Metals, London, 1987, pp. 16–18.
[24] P.M. Unterweiser, Heat Treater's Guide Standard Practices and Procedures for Steel, American Society for Metals, USA, 1982, pp. 423–426.